Coastal Engineering 188 (2024) 104443

Contents lists available at ScienceDirect

Coastal Engineering

journal homepage: www.elsevier.com/locate/coastaleng

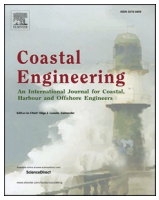

Neural Network calibration method for VARANS models to simulate wave-coastal structures interaction

Pilar Díaz-Carrasco, pilar.diaz@uca.es [a,*], Jorge Molines [b], M. Esther Gómez-Martín [b], Josep R. Medina [b]

[a] Dept. of Industrial Engineering and Civil Engineering, University of Cadiz, Avda. Ramón Puyol s/n., Algeciras (Cádiz), 11202, Spain
[b] Dept. of Transportation, Universitat Politècnica de València, Camino de Vera s/n, 46022, Valencia, Spain

ARTICLE INFO

Keywords:
Numerical modelling
IH-2VOF
VARANS equations
Mound breakwaters
Porous media
Neural Network

ABSTRACT

This study develops a calibration method for the porous media to properly model the interaction between waves and coastal structures using VARANS models. The proposed method estimates the porosity, n_p, and the optimum values of the Forchheimer coefficients, α and β, that best represent the wave-structure interaction for a complete set of laboratory tests. Physical tests were conducted in a 2D wave flume for a homogeneous mound breakwater under regular wave conditions. Numerical tests were carried out using the IH-2VOF model to simulate the corresponding physical tests and incident wave conditions (H_I, T). The numerical tests covered a wide range of Forchheimer coefficients found in the literature, α and β, and the porosity, n_p, with a total of 555 numerical tests. The results of 375 numerical tests using IH-2VOF were used to train a Neural Network (NN) model with five input variables (H_I, T, n_p, α and β) and one output variable (K_R^2). The NN model explained more than 90% ($R^2 >$ 0.90 and RMSE <5%) of the variance of the squared coefficient of reflection, K_R^2. This NN model was used to estimate the K_R^2 in a wide range of n_p, α and β, and the error (ε_a) between the physical measurements with regular waves and the NN estimations of K_R^2 was calculated. The results of ε_a as function of n_p, α and β showed that for a given porosity, n_p, it was difficult to obtain a pair of α and β values that gave a common low error if few physical tests are used for calibration. Then to calibrate properly a VARANS model it seems necessary to check the results obtained for each combination of α and β with many laboratory $\{H_I, T\}$ tests. The minimum root-mean-square error of K_R^2 (ε_{rms}) was calculated to find the optimum values of porosity and Forchheimer coefficients: n_p = 0.44, α = 200 and β = 2.825 for the tested structure. Blind tests were conducted with the remaining 180 numerical tests using IH-2VOF to validate the proposed method for VARANS models. In this study, eight or more physical tests were required to find adequate values of n_p, α and β for VARANS models related to the best performance of wave-porous structure interaction.

1. Introduction

Coastal structures are responsible for the protection from wave action of ports and highly populated coastal regions. Mound breakwaters, low-crested structures, revetments and other porous structures are commonly used to protect harbors, beaches and other highly valuable natural areas and artificial infrastructures. These coastal structures must be designed to provide safety and service during a given lifetime, and they must be designed considering the expected extreme wave conditions during lifetime. Global warming and the corresponding sea level rise (Camus et al., 2019; Reguero et al., 2019) are changing the design hypotheses, increasing overtopping rates and wave heights in the surf zone. The challenges of protecting coasts and harbors from the effects of climate change demand to understand in detail the wave-structure interaction processes for the correct design of new coastal structures and the maintenance and rehabilitation of existing ones.

The hydraulic performance and efficiency of coastal structures can be assessed in two ways, either by experimental laboratory testing or by numerical modelling. Physical experimentation is one of the best tool to analyze the wave-structure interaction. The main advantage of laboratory testing is the possibility to visualize and understand the processes occurring in the wave-structure interaction and, most importantly, the possibility to control and easily modify the physical tests. However, laboratory tests requires expensive equipment and physical facilities,

* Corresponding author.

https://doi.org/10.1016/j.coastaleng.2023.104443
Received 28 July 2023; Received in revised form 23 November 2023; Accepted 2 December 2023
Available online 11 December 2023

which are not always available. The accuracy and sampling rates are also limited and affect the quality of the experimental data (Hughes, 1993; Wolters et al., 2010). Moreover, in a laboratory plan, both in the scientific and business field, which generally requires a large number of tests to properly analyze maritime structures with design variations, the laboratory experimentation way is very expensive and time-consuming. In this case, numerical modelling arises as a useful tool to analyze the wave-coastal structure interaction, with relatively low cost and time consuming compared to a laboratory program involving many tests. The level of accuracy of numerical models is relatively high and many successful applications have been reported in reproducing the wave-structure interaction processes measured in laboratory experiments. Numerical modelling also allows non-intrusive instrumentation to be placed in the numerical model that would be intrusive in the physical model. Various types of data, such as velocity, pressure, surface elevation or turbulent kinetic energy, can be extracted from any point and time in the simulation, and the numerical instrumentation does not interfere with the flow or the structure. From a time and cost point of view, it is preferable to perform few laboratory tests to calibrate and validate a numerical model, and then use the numerical model to perform the rest of the experimental program, as well as to consider and analyze different geometry designs or wave condition scenarios.

Numerous studies use numerical models to analyze different types of coastal structures and the processes and variables involved in the wave-structure interaction; thus, Guanche et al. (2009) and Croquer et al. (2023) analyzed wave loads, Lara et al. (2011) and Moragues et al. (2020) studied the wave-breaking on the structure, and Higuera et al. (2014), Vieira et al. (2021) and Mata and Van Gent (2023) analyzed overtopping discharges. One of the main challenges in numerical modelling is the interaction of waves with the porous media of the structure. The correct modelling of the flow through the porous media is fundamental to characterize the dissipated, reflected and transmitted wave energy (Vílchez et al., 2016a; Díaz-Carrasco et al., 2020), wave-breaking on the structure, run-up and run down patterns, as well as the turbulence generated between the different layers within the structure (Clavero et al., 2020). The wave-porous structure interaction is modeled with mathematical formulations able to embrace all relevant physical processes and especially the role played by the porous media. This mathematical analysis is based on coupling two flow models: (1) the flow outside the porous media, in the outer region acting on the structure, and (2) the averaged flow through the porous media. The quality of the wave-structure modelling in numerical models depends strongly on correctly defining the wave transformation within the porous model. The representation of the flow within the porous media, characterized by a nominal diameter, D_{n50}, and a porosity, n_p, is generally based on the extended Darcy-Forchheimer equation (Forchheimer, 1901), which relies on some coefficients calibrated and validated with physical tests.

Table 1
Overview of Forchheimer coefficients (α and β) calibrated for the porous media of coastal structures characterized by a nominal diameter, D_{n50}, and a porosity, n_p.

Reference	*Structure typology*	Porous media	D_{n50} (m)	n_p	*N° of tests for calibration (porous media x physical test)*	Forchheimer coefficients α β
Van Gent (1995)	Permeable vertical breakwater	Irregular rocks	0.0610	0.442	5 × 3	1000 1.1 $\left(1+\frac{7.5}{KC}\right)$
		Semi round rocks	0.0487	0.454		
		Very round rocks	0.0488	0.393		
		Irregular rocks A	0.0202	0.449		
		Irregular rocks B	0.0310	0.388		
Liu et al. (1999)	Porous dam	Crushed rocks	0.0159	0.49	2 × 1	1000 1.1
		Glass beads	0.03	0.39		200 1.1
García et al. (2004)	Two low-crested rubble-mound breakwater	Core	0.012	0.49	2 × 1	1000 1.2
		Armor	0.039	0.53		1000 0.8
Lara et al. (2008)	Low-crested mound breakwater	Berm	0.00035	0.48	2 × 1	200 0.8
		Armor	0.035	0.50		200 1.1
Losada et al. (2008)	Rubble-mound breakwater	Core	0.01	0.48	3 × 2	200 0.8
		Filter	0.035	0.50		200 1.1
		Armor	0.135	0.50		200 0.7
Lara et al. (2011)	Porous underwater step	Rocks	0.0307	0.5	1 × 1	985.89 2.45
Lara et al. (2012)	Permeable vertical dam-break	Rocks	0.0083	0.43	1 × 1	10,000 3
Del Jesus et al. (2012)	Porous dam of Lin (1998)	Crushed stones	0.0159	0.49	2 × 1	10,000 3
		Glass beads	0.003	0.30		700 0.5
Higuera et al. (2014)	Rubble-mound breakwater of Guanche et al. (2009)	Core	0.01	0.49	4 × 1	5000 1
		Filter	0.035	0.493		5000 3
	Vertical porous breakwater	Armor	0.12	0.50		5000 2
		Rocks	0.015	0.51		20,000 1.5
Jensen et al. (2014)	Permeable vertical breakwater	Spherical glass bead A	0.002	0.34	3 × 3	500 2
		Spherical glass bead B	0.0159	0.49		500 2
		Spherical glass bead C	0.025	0.41		500 2
Pilechi et al. (2018)	Rubble-mound breakwaters	Core	0.19	0.30	3 × 0 (from literature)	200 0.7
		Armor A	0.707	0.40		200 0.8
		Armor B	1.063	0.45		200 1
Palma et al. (2019)	Rubble-mound breakwater	Core	0.002	[0.4, 0.5, 0.6]	3 × 3	1000 1.1
		Filter	0.02	[0.5, 0.6, 0.7]		1000 1.1
		Armor	0.04	[0.7, 0.6, 0.8]		1000 1.1
Molines et al. (2019, 2020)	Mound breakwater with crown wall	Core	0.007	0.4	3 × 0 (from literature)	200 1.1
		Filter	0.017	0.4		200 1.1
		Armor	0.0382	0.4		200 1.1
This study	Homogeneous Mound breakwater	Rocks	0.030	[0,37, 0.46]	1 × 25	200 2.825

Although there are a variety studies in the literature analyzing the porous flow characteristics in coastal engineering applications, the problem of the wave interaction with the porous structures has not been solved yet. Firstly, different authors have proposed Forchheimer coefficients, α and β, in a wide range of values for the same wave conditions and coastal structure typologies (see Table 1 in Section 2). There is a large uncertainty in selecting the adequate values for these coefficients (α and β) to correctly model the flow through the porous media of a structure. Secondly, the measurement of the porosity, n_p, is not easy as porosity may slightly change during the laboratory tests, and "in situ" measurement is almost impossible; therefore, the physical measurement of structure porosity is not reliable. The scatter of the measured n_p may be due to the expansion in the water and rearrange of the granular units by the physical model construction in a wave flume or basin and/or during the wave impact with the structure.

The main objective of this study is to develop a method to estimate the most appropriate Forchheimer coefficients, α and β, and porosity, n_p, to correctly model the interaction between waves and coastal structures using Volume-Averaged Reynold Averaged Navier-Stokes (VARANS) equations numerical models. The calibration method provides the optimum values of the Forchheimer coefficients and the porosity from the error prediction of a Neural Network (NN) model developed using physical and numerical tests. Physical tests were conducted at the University of Granada for a homogeneous mound breakwater under regular waves, non-overtopping and non-breaking conditions. Numerical tests were conducted to reproduce the physical tests using the IH-2VOF model (Lara et al., 2008), with different combinations of porosity and Forchheimer coefficients. A total of 555 numerical tests using IH-2VOF were calculated, and 375 of them were used to develop the NN model. To calibrate the porous media, the proportion of the reflected wave energy, K_R^2, was compared between the physical and numerical tests estimated with the NN model. Results corresponding to the remaining 180 numerical tests of IH-2VOF were used for blind testing to validate the method.

This paper is structured as follows. Section 2 includes a literature review on modelling the wave interaction with the porous media of coastal structures, paying attention to the mathematical formulation, calibrated Forchheimer coefficients and methods. Section 3 describes the physical laboratory tests and numerical tests using the IH-2VOF model. Section 4 develops the NN model to estimate errors for different combinations of H_I, T, n_p, α and β. The procedure to find the optimum values of the Forchheimer coefficients, α and β, and the porosity, n_p, is described in Section 5. The proposed method to calibrate n_p, α and β is described in Section 6, as well as the recommended minimum number of tests required to use this method efficiently. Section 7 presents the summary and some conclusions derived from this study.

2. Literature review on modelling the porous media of coastal structures

The porous media modelling is usually a complex task (irregular pores and variable shapes and sizes), which are often assumed to be a rigid structure. There is no unique way to simulate the flow through the porous media, but existing approaches given in the literature are mostly based on Navier-Stokes (NS) equations; a detailed description of the different approaches can be found in Losada et al. (2016). The flow outside the porous media is usually solved by Reynolds-Averaged Navier-Stokes (RANS) equations, which are the time averaged of NS equations, with an appropriate turbulence model. For coastal structures, the flow through its porous media is frequently modeled using a macroscopic approach, which calculates the mean behaviour of the flow averaging their properties inside a continuous porous media. In particular, most numerical models solving the flow through the porous media are based on Volume-Averaged Reynold Averaged Navier-Stokes (VARANS) equations.

The VARANS equations are derived by integrating the RANS equations over a Control Volume. Their final form is shown in Eqs. (1) and (2). A more detailed derivation of VARANS equations can be found in Jensen et al. (2014).

$$\nabla \overline{u} = 0 \tag{1}$$

$$\frac{\partial}{\partial t}\frac{(\rho \overline{u})}{n_p} + \frac{1}{n_p}\nabla \bullet \left(\frac{1}{n_p}\rho \overline{u} \times \overline{u}\right) = -\nabla p + \frac{1}{n_p}\nabla(\nu \nabla \bullet \overline{u}) + \rho \overline{f_b} - I \tag{2}$$

where $\overline{u}$ is the velocity vector, p is the wave pressure, ρ is the water density, ν is the kinematic viscosity, n_p is the porosity, $\overline{f_b}$ represents the body forces, namely gravity; and I is the hydraulic gradient, which represents the flow resistance forces inside the porous media by the extended Forchheimer equation:

$$I = a\overline{u} + b\overline{u}|\overline{u}| + c_A \frac{\partial(\rho \overline{u})}{\partial t} \tag{3}$$

being a, b and c_A, coefficients related to the porous flow, with dimensions of s/m, s^2/m^2 and s^2/m, respectively. In Eq. (3), the first term is the linear term of the drag force that represents a Darcy's flow or laminar flow behavior, the second term is the non-linear term of the drag force that considers the fully turbulent flow behavior, and the last term is the inertial force due to the effect of added mass (Polubarinova-Kochina, 1962). The added mass defines the extra momentum needed to accelerate the same volume of water in a porous media (Van Gent, 1995). Several approaches to determine a, b and c_A, can be found in literature. Ergun (1952), Engelund (1953), Van Gent (1995) and Burcharth and Andersen (1995), among others, analyzed these coefficients and established relationships with the flow conditions for different hydraulic regimes (Losada et al., 2016). The following analytical expressions to calculate a, b and c_A are the most commonly used:

$$a = \alpha \frac{(1-n_p)^2}{n_p^3}\frac{\mu}{D_{n50}^2} \tag{4}$$

$$b = \beta\left(1 + \frac{7.5}{KC}\right)\frac{(1-n_p)}{n_p^3}\frac{\rho}{D_{n50}^2} \tag{5}$$

$$c_A = \gamma_p \frac{(1-n_p)}{n_p} \tag{6}$$

where D_{n50} is the granular nominal diameter, μ the dynamic viscosity, KC is the Keulegan-Carpenter number that accounts for the transient nature of flows, and α, β and γ_p are three empirical coefficients. According to Losada et al. (2008) and Higuera et al. (2014), the empirical coefficient γ_p has a very small influence and yields good results with a constant value of $\gamma_p = 0.34$. The values of α and β are coefficients which need to be calibrated.

Numerous studies calibrated the Forchheimer coefficients, α and β, considering laboratory tests and numerical VARANS models to describe wave-structure interaction, such as, overtopping, wave pressure, wave energy transformation, wave-breaking on the slope and armor stability. Table 1 shows some of the studies that used VARANS numerical modelling and calibrated α and β values for different typologies of coastal structures, mainly breakwaters characterized by different porous layers with a nominal diameter, D_{n50}, and a porosity, n_p. The value of the porosity provided by the studies listed in Table 1 is physically measured in laboratory (Van Gent, 1995), or assumed values depending on the nominal diameter, D_{n50}, and following manual recommendations (CIRIA/CUR/CETMEF, 2007; Vílchez et al., 2016b). The number of physical tests used to calibrate the Forchheimer coefficients, is gathered in Table 1.

Table 1 shows different values of α and β given by researchers depending on how these coefficients were determined or calibrated.

There are many more wave-porous structure interaction modelling studies that calibrate the Forchheimer coefficients with the same method and in the same range of values as the studies presented in Table 1. Recent studies developed other calibration methods for α and β using numerical techniques or simplified expressions instead of experimental calibration. For example, Vílchez et al. (2016b) used the simplified Forchheimer equation (Eq. 3) of Sollitt and Cross (1972), based on the Lorentz's hypothesis of equivalent work, and determined a non-dimensional linear friction coefficient that calibrates the flow inside the porous media of several breakwater typologies. Zhao et al. (2021) calibrated the Forchheimer coefficients, α and β, for a porous vertical structure and a rubble-mound breakwater using the calibration method of Zhao et al. (2019), which relates α and β values with the wave damping rate. Vieira et al. (2021) presented a Neural Network model that determined the optimum combination of Forchheimer coefficients to numerically predict the mean overtopping discharges. They used a database to develop the NN model based on limited numerical cases simulated in the IH-2VOF model which solves VARANS equations, with few values of β in the range [0.8, 1.2] for each porous layer of the structure, and a constant linear coefficient, $\alpha = 200$. Norouzi et al. (2022) used the Particle Swarm Optimization (PSO) algorithm to optimize a, b and c_A coefficients in non-Darcy steady and unsteady flow conditions in a rockfill installed inside a wave tank. Dang et al. (2023) determined the Forchheimer coefficients in a thin perforated plate using an advanced machine learning algorithm based on decision trees of GBDT method. They tested 72 samples with only 3 wave conditions, H and T, three values of α, and four values of β in combination with two porosities.

Despite the numerous numerical modelling studies of coastal structures using the Forchheimer coefficients, the wide range of values found in the literature, $200 \leq \alpha \leq 20{,}000$ and $0.4 \leq \beta \leq 4$, and the scatter of the porosity, n_p, is a clear indication of the need of a robust method to calibrate n_p, α and β. The calibration method used in most studies using numerical VARANS models are based on a few physical tests; usually, the porosity, n_p, is fixed and the different values of α and β are considered in a limited range, until a few experimental results somehow resemble the numerical ones.

3. Physical and numerical tests

This section describes the 2D physical and numerical tests used in this study to calibrate the Forchheimer coefficients, α and β, and the porosity, n_p, to model the interaction between waves and a coastal structure.

3.1. Physical experiments

2D physical tests were conducted by Díaz-Carrasco (2019, 2023) in the wave flume with 23 m long, 0.65 m wide and 1 m deep of the Fluid Dynamics Laboratory at University of Granada, Spain. The physical model was a homogeneous mound breakwater with a G_c (m) = 0.24 crest width, a breakwater height F_{MT} (m) = 0.55, and seaward and landward slope H/V = 2/1 and H/V = 3/2, respectively. The porous media is a homogeneous rock material with a nominal diameter D_{n50} (m) = 0.030, rock mass density ρ_s (g/cm^3) = 2.64, and a porosity measured in laboratory, n_p, = 0.46 according to manual recommendations (CIRIA/CUR/CETMEF, 2007); Fig. 1 shows the cross section of the physical model.

The physical tests were carried out using regular waves under non-overtopping and non-breaking wave conditions. A total of $N_T = 37$ physical tests with regular waves were tested at laboratory with $N_w = 100$ waves per test. The physical tests were reproduced later numerically with the IH-2VOF model. Table 2 describes the target wave conditions tested in the laboratory; being H_I and T the incident wave height and wave period, and L is the wavelength calculated by the linear dispersion equation, h/L is the relative water depth, H_I/L is the wave steepness, and

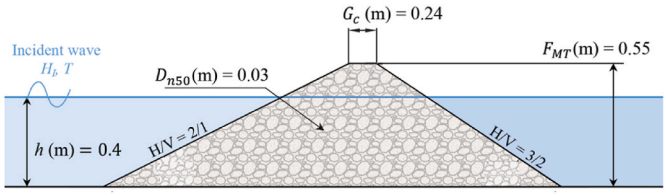

Fig. 1. Cross section of the physical model of the homogeneous mound breakwater tested.

Table 2
Range of wave variables tested in the laboratory.

Variables	*Range [Min, Max]*
h (m)	0.4
T (s)	[1.02, 3.64]
H_I (m)	[0.02, 0.12]
(h/L)	[0.06, 0.28]
(H_I/L)	[0.01, 0.03]
R_{ec}	[100, 940]

$R_{ec} = \frac{\left(\frac{n_p \cdot H_I}{T}\right) D_{n50}}{\nu}$ the Reynolds number of the porous media. R_{ec} characterizes the hydrodynamic regime inside the porous media, a region where the laminar, turbulent and inertia forces are relevant to describe the water flow (Gu and Wang, 1991; Van Gent, 1995; Burcharth and Andersen, 1995). The experimental technique consisted in varying H_I/L for each fixed value of h/L, taking into account the conditions of paddle generation and the imposed non-overtopping and non-breaking conditions. The experimental technique is described in detail in Díaz-Carrasco (2019). The AwaSys software package was used to generate waves with the active wave absorption system (AWACS®)to eliminate re-reflected waves in the wave flume; additionally, a dissipative parabolic ramp was placed at the end of the flume to minimize the wave reflection of the flume. The water depth in the wave flume was constant, h (m) = 0.4.

Fig. 2 shows a scheme of the longitudinal cross section of the wave flume and the resistance wave gauges (G) located along the flume to measure the water surface elevation with a sampling frequency of 20 Hz. The incident and reflected waves were estimated with the wave records taken by gauges G1, G2 and G3. The incident and reflected wave trains were separated using the method of Baquerizo (1995), which provides the squared coefficient of reflection, K_R^2, and phase, φ_R, of the reflected waves. The transmission coefficient, K_T^2, was computed from the records of wave gauge G5; K_T^2 was not used in this study. A detailed analysis of the experimental tests and the $[K_R^2, K_T^2]$ values measured in each test (H_I/L, h/L) is given in Díaz-Carrasco (2023). Specifically, the range of K_R^2 values measured in the laboratory was $K_R^2 = [0.026–0.41]$.

3.2. Numerical experiments

3.2.1. Model description

The IH-2VOF numerical model (Losada et al., 2008) was used in this study to model the interaction between waves and the porous breakwater tested at laboratory, since it is able to simultaneously solve the flow both inside and outside the porous media. IH-2VOF solves the two-dimensional Reynolds Averaged Navier-Stokes (RANS) equations

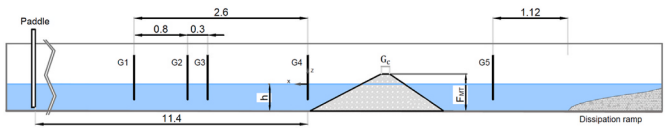

Fig. 2. Longitudinal cross section of the wave flume and location of wave gauges (dimensions in meters).

outside the porous media using the $k-\epsilon$ turbulent model to calculate the kinetic energy (k) and the turbulent dissipation rate (ϵ). The free-surface is tracked by the Volume of Fluid (VOF) method (Hirt and Nichols, 1981). The flow through the porous media is solved by the Volume-Averaged Reynolds Averaged Navier-Stokes (VARANS) equations (see Eqs. (1) and (2) in Section 2).

IH-2VOF model has been applied to study numerous wave-structure interaction problems including low-crested mound breakwaters (García et al., 2004; Lara et al., 2006), composite and emerged breakwaters (Lara et al., 2008; Guanche et al., 2009), wave energy transformation on a wide range of porous breakwaters typologies (Vílchez et al., 2016b), wave-breaking on porous structures (Del Jesus et al., 2012), wave-overtopping on rubble-mound breakwaters (Vieira et al., 2021), pore-pressure on rubble mound breakwater (Guanche et al., 2015), and wave energy conversion on non-conventional rubble mound and vertical breakwaters (Di Lauro et al., 2019; 2020).

3.2.2. Numerical set-up

A 2D domain of the wave flume described in Fig. 2 was reproduced in the IH-2VOF model. The numerical domain was slightly shorter in the x-direction (15.6 m long) than the wave flume as the dissipation ramp was substituted by an active absorption condition to reduce the number of cells. A mesh sensitivity analysis was performed to assess the computational cost and the accuracy of the results, comparing the measured in laboratory and numerically obtained wave height far from the region of the structure for different mesh sizes. A uniform mesh on the y-direction was used with a grid cell size of 0.5 cm $\approx \Delta_y = H/10$. The x-direction was divided in 2 subzones as defined in Fig. 3a: (1) the 10.4 m-long outer region corresponding to the wave generation zone with a cell size of 2 cm $\approx \Delta_x = L/100$, (2) the region corresponding to the breakwater (wave-structure interaction), where higher accuracy is needed, with a cell size of 1 cm. The total number of cells in the numerical domain was 1 017 (x-direction) x 201 (y-direction). The active wave absorption condition was considered at the generation boundary and at the end of the domain to reproduce the same conditions as in the laboratory experiments, i.e., to avoid wave reflection at boundaries (see Fig. 3b). Numerical wave gauges G01 to G05 correspond to the physical wave gauges G1 to G5.

The porous structure was modeled in the IH-2VOF model using the physical characteristics, D_{n50} and n_p, and the Forchheimer coefficients: α, β and γ_p. The physical homogeneous breakwater model with D_{n50} (m) = 0.03 was reproduced in the numerical model considering different combinations of n_p, α and β. The value of $\gamma_p = 0.34$ (Van Gent, 1995) was assumed to be invariable because the results are practically insensitive to its variation (Losada et al., 2008; Higuera et al., 2014). To cover the full range of α and β values used in the literature (Table 1), this study considered the following range parameters given in the literature: $200 \leq \alpha \leq 20{,}000$ and $0.4 \leq \beta \leq 4.0$. As discussed in Section 1, the porosity measurement at laboratory is not reliable; thus, the porosity (n_p) was considered in this study as an additional parameter to be calibrated. The

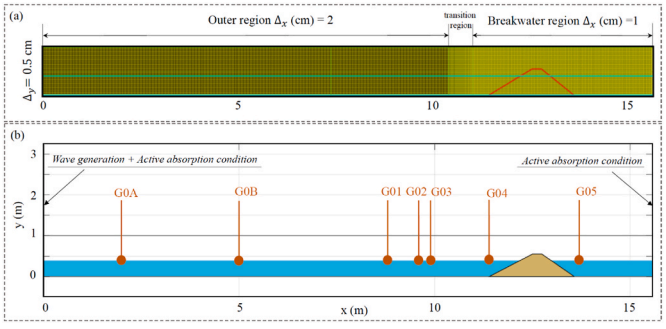

Fig. 3. Numerical domain in IH-2VOF model: (a) mesh grid, (b) wave gauges position.

porosity values were chosen in the range $0.37 \leq n_p \leq 0.46$, which corresponds to the possible porosities for homogeneous stones of size D_{n50} (m) = 0.03 following the recommendations of CIRIA/CUR/CETMEF (2007).

The incident wave height, H_I, and wave period, T, obtained from the temporal analysis of the $N_T = 37$ physical tests of regular waves (see Table 2) were numerically generated with the same number of waves per test, $N_w = 100$. For each test ($i = 1, \ldots, 37$), $N_R = 15$ numerical simulations were conducted and a random combination of $\{n_p, \alpha, \beta\}$ for each "r" simulation ($r = 1, \ldots, 15$) was selected within the ranges: $0.37 \leq n_p \leq 0.46$, $200 \leq \alpha \leq 20{,}000$ and $0.4 \leq \beta \leq 4.0$. The different values of n_p, α and β for each "i" physical test and "r" simulation were randomly obtained with the following relations,

$$n_{p_{ir}} = n_{pmin} + U(0,1)_{ir} \bullet \left(n_{pmax} - n_{pmin}\right);\ \text{being}\ \ n_{pmax} = 0.46, n_{pmin} = 0.37 \tag{7a}$$

$$\alpha_{ir} = \exp\left[\ln \alpha_{min} + U(0,1)_{ir} \bullet (\ln \alpha_{max} - \ln \alpha_{min})\right];\ \text{being}\ \alpha_{max} = 20{,}000,\ \alpha_{min} = 200 \tag{7b}$$

$$\beta_{ir} = \beta_{min} + U(0,1)_{ir} \bullet (\beta_{max} - \beta_{min});\ \text{being}\ \beta_{max} = 4.0, \beta_{min} = 0.4 \tag{7c}$$

in which $\{n_{p_{ir}}, \alpha_{ir}, \beta_{ir}\}$ are the porosity and Forchheimer parameters corresponding to the "i" physical test and "r" simulation ; and $U(0,1)$ is a random number uniformly distributed in the range [0,1]. Fig. 4 shows a scheme of the methodology described above with a total of N_T x $N_R = 37 \times 15 = 555$ combinations of $\{n_p, \alpha, \beta\}$ different from each other and 555 numerical tests using IH-2VOF. The random selection and combinations made to simulate the cases in IH-2VOF model will allow to develop a Neural Network (NN) model (see Section 4) trained with all possible combinations in the sample space $\{H_I, T, n_p, \alpha \text{ and } \beta\}$, and thus to avoid a NN model biased by pre-defined combinations and to help the correct NN model interpolation. The computer time for each numerical test using IH-2VOF varied between 20 min and 2 h in a personal computer with Eight-Core and processor of 3.70 GHz. For computational efficiency, most tests were simultaneously run in the RIGEL Computational Cluster at the Universitat Politècnica de València (Spain), it required few days to simulate the 555 numerical VARANS tests.

Numerical wave gauges were placed in the same location as the ones

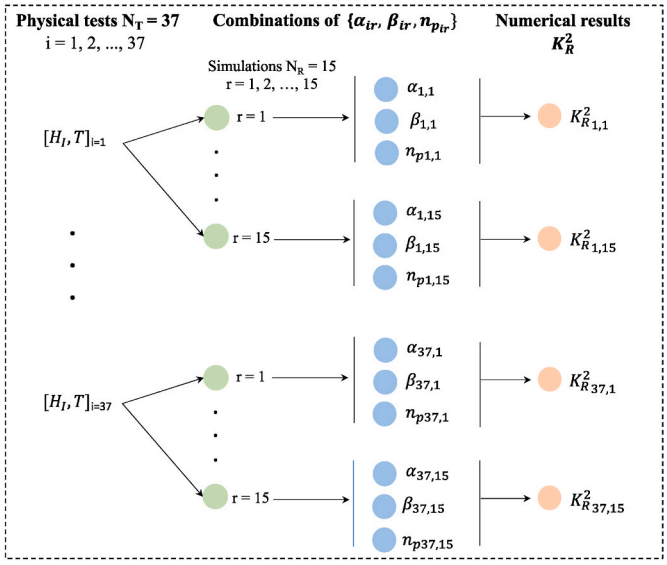

Fig. 4. Scheme of the numerical tests simulated using the IH-2VOF model. The number of physical test is represented by subindex $i = 1, \ldots, 37$ and for each test "i", $r = 1, \ldots, 15$ simulations were conducted with a random combination of $\{n_p, \alpha, \beta\}$ obtained by Eqs. (7a), (7b) and (7c), respectively. A total of N_T x $N_R = 37 \times 15 = 555$ numerical cases and numerical K_R^2 results were obtained.

used in the laboratory experiments (see Fig. 3b). Two additional wave gauges G0A and G0B were located near the generation zone to analyze the mesh sensitivity and the numerically generated waves; the time step was Δ_t= 0.05 s, in agreement with the sampling frequency of the wave gauges in the physical tests. The methodology to calculate {H_I, T, L} and K_R^2 for the 555 numerical tests was similar the same used for the 37 physical tests.

4. Neural Network model for estimating wave reflection

In this section a Neural Network (NN) model is developed in order to predict K_R^2 on the homogeneous mound breakwater using the numerical results with the {n_p, α, β} combinations from the IH-2VOF model. Once the NN is trained, K_R^2 can be estimated much faster than any numerical VARANS model. The NN can then be used as an auxiliary numerical tool to estimate K_R^2 and calibrate the values of n_p, α and β for the tested breakwater within the ranges of the IH-2VOF tests.

4.1. Neural Network structure

This section describes the NN model developed from the results corresponding to the 555 numerical tests using IH-2VOF to estimate the proportion of reflected wave energy, K_R^2 in homogeneous mound breakwaters. Fig. 5 represents the NN model with five input variables (N_I = 5), 20 hidden neurons (N_H = 20) and one output variable (No = 1). For the porous media of the breakwater characterized by a D_{n50}, the selected input variables were: H_I, T, n_p, α and β. The output variable was the squared coefficient of reflection, K_R^2.

The number of parameters of this NN model was P=N_O + N_H(N_I + N_O +1) = 1 + 20 (5 + 1 + 1) = 141. Although a total of N_T x N_R = 37 × 15 = 555 numerical tests using IH-2VOF were available, only 25 physical tests (randomly selected from the total 37 tests) with their corresponding combination of {n_p, , β}, that is 25 × 15 = 375 numerical tests were considered to build up the NN model. The results from the remaining 12 × 15 = 180 numerical tests were used only for a final blind test.

The NN model was trained and tested using the NN toolbox (Beale et al., 2019) in the MATLAB® environment (MATLAB, 2022) with the following characteristics:

(1) Early stopping criterion to prevent overlearning,
(2) Randomly selection of data using 263 cases (70%) for training, 56 cases (15%) for validation and 56 cases (15%) for testing,
(3) Levenberg-Marquardt training algorithm, and
(4) hyperbolic tangent sigmoid transfer function for hidden neurons.

4.2. Neural Network performance

Fig. 6 shows the comparison between the K_R^2 predicted by the NN model and the K_R^2 calculated with IH-2VOF model. The coefficient of determination, R^2, and the root-mean-squared error, RMSE, were used in this study to measure the goodness of fit of the NN model for training, validation and testing. The higher R^2 or lower RMSE, the better is the prediction of K_R^2 given by the NN model compared to the numerical IH-2VOF model. The coefficient of determination and the root-mean-squared error are given by,

$$R^2 = 1 - \frac{\sum_{m=1}^{M} (Y_{Vm} - Y_{NNm})^2}{\sum_{m=1}^{M} (Y_{Vm} - \overline{Y_V})^2}; \tag{8a}$$

$$\mathrm{RMSE} = \sqrt{\frac{\sum_{m=1}^{M} (Y_{Vm} - Y_{NNm})^2}{M}} \tag{8b}$$

where Y_V is the K_R^2 from IH-2VOF model (K_{RVOF}^2), Y_{NN} is K_R^2 from NN model (K_{RNN}^2), $\overline{Y_V}$ is the mean value of Y_V; M = 25 × 15 = 375 is the total number of cases and "m" is the data index (m = 1, 2, …M).

The NN model with five input parameters {H_I, T, n_p, α, β} predicted very well the numerical results of IH-2VOF model (see Fig. 6), with R^2 = 0.99 and RMSE = 2.1% for training data, R^2 = 0.99 and RMSE = 1.7% for validation, and R^2 = 0.92 and RMSE = 4,6% for testing. This NN model is computationally much faster than IH-2VOF model and can be used as an auxiliary tool to find the best combination of {n_p, α, β}.

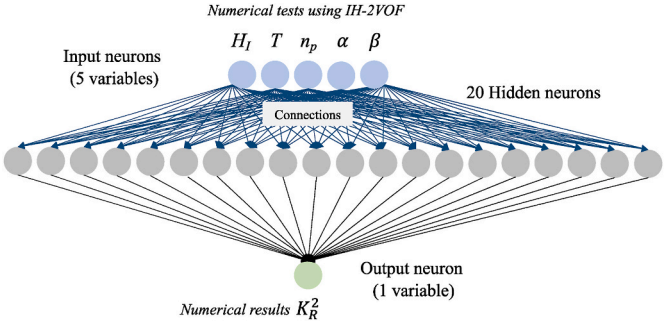

Fig. 5. Scheme of the NN model using the 375 numerical tests using IH-2VOF model.

5. NN model results

This section presents the estimations of the porosity and Forchheimer coefficients using the NN model as an auxiliary numerical tool to estimate K_R^2 and to compare them with K_R^2 measurements from physical tests. Then, the optimum combination of {n_p, α, β}, which calibrates the porous media of the tested homogeneous mound breakwater, is calculated.

5.1. Estimations of porosity and forchheimer coefficients for each test

Because of the computational efficiency of the NN model trained with numerical results from IH-2VOF model, a huge number of combinations of n_p, α and β for each tested pair {H_I,T} were considered to obtain many numerical estimations of K_R^2. The estimation of K_R^2 using the NN model, named K_{RNN}^2, was compared with the K_R^2 measurements from physical tests, named K_{RLAB}^2, to calibrate the parameters of the porous media (n_p, α and β) of the homogeneous mound breakwater. The procedure was the following:

(1) Selection of combinations of the five input variables {H_I, T, n_p, α, β} (see Fig. 7) covering uniformly the range of variables found in the literature (Table 1):
   - o N_T = 25 pairs of {H_I, T} were taken from the 25 physical tests previously selected to develop the NN model (physical tests of Section 3.1).
   - o N_{np} = 19 values of porosity (n_p) were considered, with a constant step in the range [0.370, 0.460]; n_p = 0.370; 0.375; …; 0.455; 0.460.
   - o N_α = 200 values of α were considered, with a logarithmic step in the range [200, 20,000]; α = 200; 204.68; …; 19,542; 20,000.
   - o N_β = 721 values of β were considered, with a constant step in the range [0.400, 4.000]; β = 0.400; 0.405; …; 3.955; 4.000.
(2) Estimation of the output variable K_R^2 using the NN model, K_{RNN}^2, for the N_T x N_{np} x N_α x N_β = 25 × 19 x 200 × 721 = 68,495,000 different combinations of the five input variables {H_I, T, n_p, α, β}.

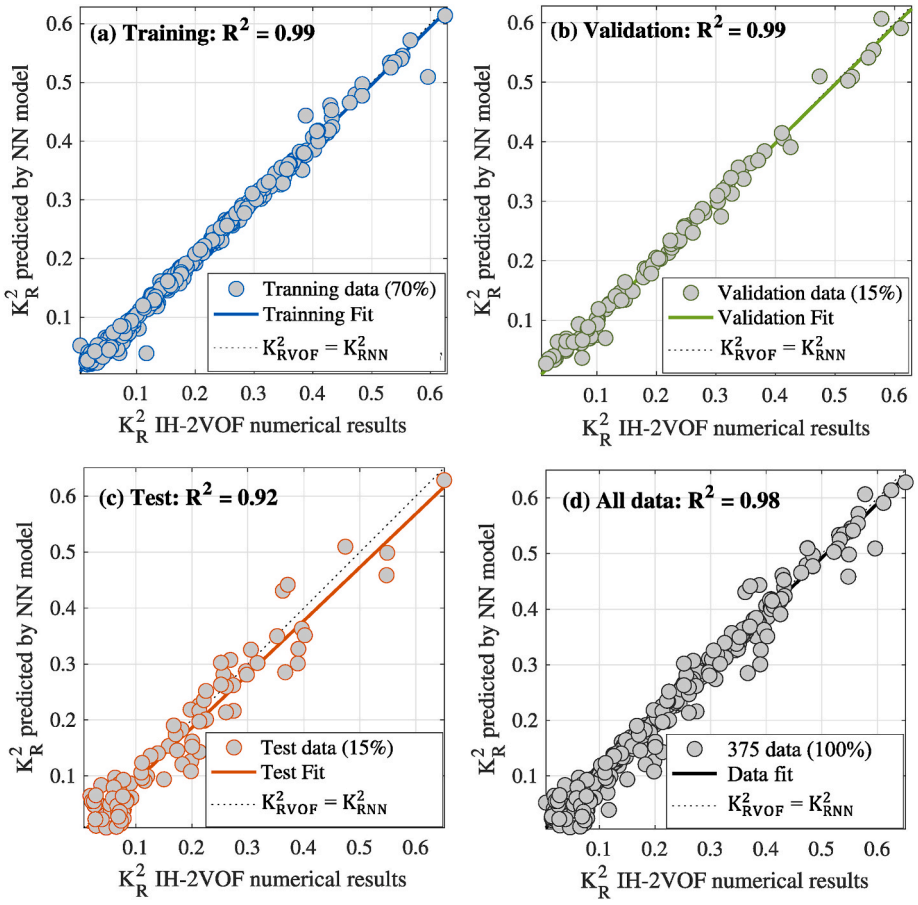

Fig. 6. Comparison between the K_R^2 predicted by the NN model (K_{RNN}^2) and the 375 results of K_R^2 calculated with IH-2VOF model (K_{RVOF}^2). NN model fits for: (a) 263 training data (70 %), (b) 56 validation data (15%), (c) 56 test data, and (d) 375 data (100 %).

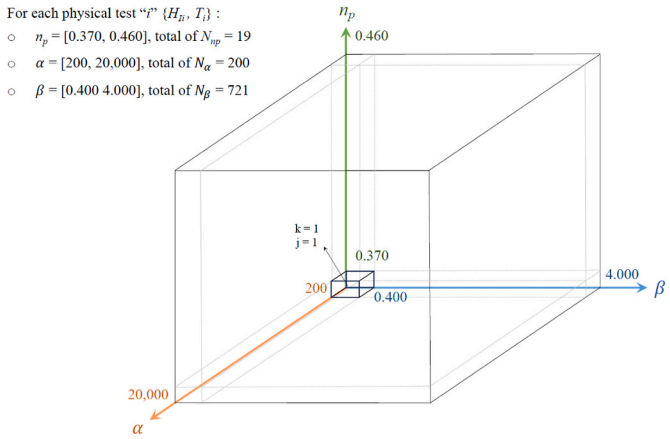

Fig. 7. Scheme of the selection of the five input variables $\{H_I, T, n_p, \alpha, \beta\}$ combined in a homogeneous cloud with a total of 25 × 19 x 200 × 721 = 68,495,000 numerical cases simulated in the 3D space of $\{n_p, \alpha, \beta\}$.

(3) Comparison of the NN estimations of the squared reflection coefficient, K_{RNN}^2, with the physical measurements, K_{RLAB}^2. The absolute error was calculated as,

$$\varepsilon_{a_{kij}}\left(K_R^2\right) = \left|K_{RLAB_i}^2 - K_{RNN_{kij}}^2\right| \tag{9}$$

where sub-index "*i*" ($i = 1, \ldots, 25$) refers to physical tests, "*k*" ($k = 1, \ldots, 19$) refers to porosity, and "*j*" ($j = 1, \ldots, 200 \times 721$) refers to different pair of $\{\alpha,\beta\}$ values for a given porosity (n_p) and physical test (H_I, T). Note that Eq. (9) can emphasize the error for small measured K_{RLAB}^2 values.

Fig. 7 shows a scheme of a homogeneous cloud of N_{np} x N_α x N_β = 2,739,800 points $\{n_p, \alpha, \beta\}$ in a 3D space; each point considers 25 pair of $\{H_I, T\}$ corresponding to the 25 physical tests used for calibration. For each physical test "*i*" $\{H_I, T\}$ and each porosity "*k*", a pair "*j*" of $\{\alpha, \beta\}$ values was selected.

Fig. 8 represents the results of the absolute errors, ε_a (Eq. (9)), expressed as a percentage, for each pair of α (x-axis) and β (y-axis) according to the NN estimations for two porosities (n_p = 0.38 and 0.45) and two physical tests: (1) H_{I1} (m) = 0.03, T_1 (s) = 1.12 (Fig. 8a and b), and (2) H_{I2} (m) = 0.10, T_2 (s) = 2.46 (Fig. 8c and d). The minimum value of ε_a for each case is marked with a red circle. Assuming a constant porosity for the numerical model, the optimum values$\{\alpha, \beta\}$ with minimum value of ε_a are different for each test $\{H_I, T\}_i$. For example, if n_p = 0.38 (Fig. 8a and c), the minimum errors were given by α = 4341 and 802, and β = 3.745 and 2.695 for $\{H_{I1}, T_1\}$ and $\{H_{I2}, T_2\}$, respectively. For the same test $\{H_{Ii}, T_i\}$, the minimum error corresponds to optimum values of $\{\alpha, \beta\}$ which are different depending on the porosity. For example, for $\{H_{I2}, T_2\}$ (Fig. 8b and d), the minimum was obtained with α = 802 and 1,761, and β = 2.695 and 3.925 for n_p = 0.38 and n_p = 0.45, respectively.

The results obtained in this section are pointing out that selecting one or a few physical tests $\{H_I, T\}$ to calibrate the values of n_p, α and β (as reported in the literature) is not sufficient to obtain the best representation of the hydraulic performance of wave-porous structure interaction. Therefore, for the calibration of a VARANS model, with or without the using of a NN model, it seems necessary to check the results obtained

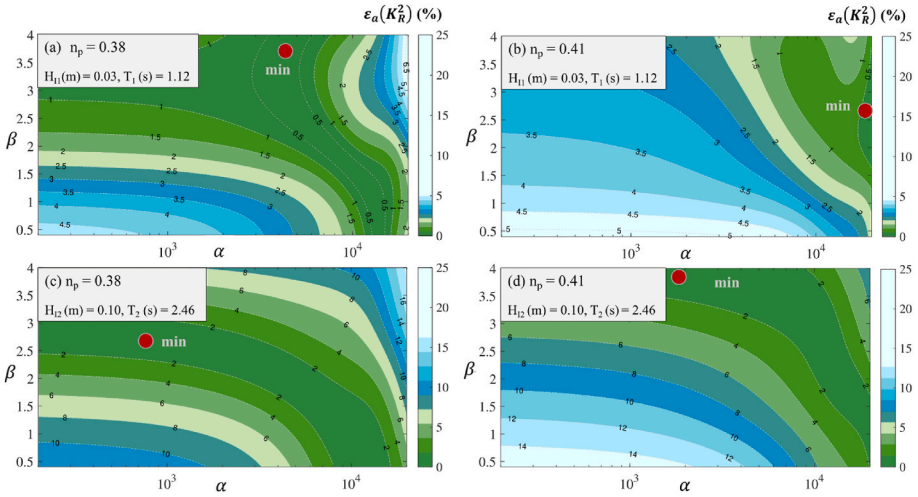

Fig. 8. Results of the absolute error, $\varepsilon_a\ (K_R^2)$ %, calculated with Eq. (9), for each pair of α (x-axis) and β (y-axis) according to the NN estimations for two porosities, n_p = 0.38 and 0.45, and two tests: (a, b) H_{I1} (m) = 0.03, T_1 (s) = 1.12; (c, d) H_{I2} (m) = 0.10, T_2 (s) = 2.46. The minimum error is marked with a red circle.

for each combination of {α, β} with many laboratory {H_I, T} tests.

5.2. Optimum values for porosity and forchheimer coefficients (n_p, α, β)

The previous section calculates values of n_p, α and β which gave a minimum error between the K_R^2 estimated by NN and the measured in laboratory for each physical test {H_I, T}$_i$. However, as observed in previous studies found in the literature and for greater computational efficiency, an optimum combination of n_p, α and β for all physical tests related to the best performance of wave-porous structure interaction should be calculated. For that, the NN estimations for each combination of {n_p, α, β} common to all 25 physical tests were compared with the measured result of the physical test as follow: for each porosity, "k" and for each pair "j" of {α, β}, the root-mean-square error (ε_{rmskj}) between the NN estimations and measurements of K_R^2 from the 25 physical tests were calculated as,

$$\varepsilon_{rmskj}\left(K_R^2\right) = \sqrt{\frac{\sum_{i=1}^{25}\left(K_{RLAB}^2 i - K_{RNN}^2 kij\right)^2}{25}} \tag{10}$$

A total of 19 × 200 x 721 = 2,739,800 root-mean-square errors, ε_{rmskj}, were calculated. Each value of ε_{rmskj} is characteristic of a {n_p, α, β} combination for all 25 physical tests. Fig. 9a shows the empirical Cumulative Distribution Function (eCDF) of ε_{rms} results for all the combinations of {n_p, α, β}. The lowest percentiles of the eCDF corresponded to small errors between estimations K_{RNN}^2 and measured K_{RLAB}^2 with {n_p, α, β} combinations in an increasingly restricted range. For example, the 5% percentile has low errors, $\varepsilon_{rms} \leq 2.5$ %, and the combinations of {n_p, α, β} were in a cloud of points within the restricted range: $0.39 \leq n_p \leq 0.46$, $200 \leq \alpha \leq 8100$ and $1.3 \leq \beta \leq 3.5$. Fig. 9b represents the range of {n_p, α, β} values for a small error, $\varepsilon_{rms} \leq 2.5$ %. Fig. 9b shows that there is a correlation between α and β values for a fixed porosity (Higuera et al., 2014): for a constant porosity, $n_p = 0.46$, in the cloud of points with low errors $\varepsilon_{rms} \leq 2.5$ %, if α increases then β has to decrease (and vice versa) to find the pair of α and β values that represents better the flow inside the porous media of the structure, that is, {$\alpha = 8100$ and $\beta = 1.3$}, and {$\alpha = 200$ and $\beta = 3.5$}. The percentile 0.5% has a value of $\varepsilon_{rms} < 2.30$ %, and the combinations of {n_p, α, β} were even in a highly restricted range, with the same correlation between α and β: $n_p = 0.44$, $200 \leq \alpha \leq 276$ and $2.805 \leq \beta \leq 2.830$. As the error, ε_{rms}, decreases the range of values of {n_p, α, β} becomes smaller. For the 90 % percentile, the NN model provided estimations K_{RNN}^2 far from that measured K_{RLAB}^2 in the physical tests with $\varepsilon_{rms} \geq 14.4$ %.

Small errors in Fig. 9a have a range of {n_p, α, β} values that would be adequate to calibrate the porous media and would represent the wave-structure interaction for all laboratory tests. To obtain an optimum combination of {n_p, α, β} for all physical tests related to the best performance of wave-porous structure interaction, the minimum value of ε_{rms} was calculated, equal to $\varepsilon_{rms} = 2.28$ %. This minimum ε_{rms} value between the NN estimations and laboratory measurements of K_R^2 for the 25 physical tests corresponded to an optimum and unique combination:

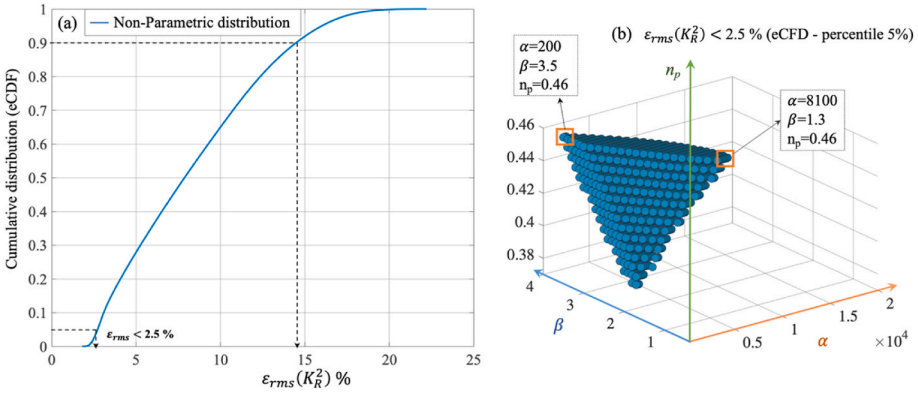

Fig. 9. (a) Cumulative Non-Parametric distribution (eCDF) of the root-mean-square errors, $\varepsilon_{rms}(K_R^2)$ %, calculated by Eq. (10) for all combinations of {n_p, α, β}; (b) n_p, α and β values with $\varepsilon_{rms}(K_R^2) \leq 2.5$ % (percentile 5% of the eCDF).

$n_p = 0.44$, $\alpha = 200$ and $\beta = 2.825$. The porosity $n_p = 0.44$ was selected in the range $0.37 \leq n_p \leq 0.46$, the linear coefficient $\alpha = 200$ was selected in the range $200 \leq \alpha \leq 20{,}000$ and the non-linear coefficient $\beta = 2.825$ was selected in the range $0.400 \leq \beta \leq 4.000$. The selection of $\alpha = 200$ in this study, the lowest range limit found in the literature, is pointing out the need to explore the range $\alpha < 200$ in the calibration process of Forchheimer coefficients. The NN was not able to give $\alpha < 200$ since it was trained in the range $200 \leq \alpha \leq 20{,}000$.

Because of the NN model emulates the numerical IH-2VOF model, the calibrated porosity and Forchheimer coefficients ($n_p = 0.44$, $\alpha = 200$, $\beta = 2.825$) obtained in this study are adequate to characterize the interaction between the waves and the porous media of the tested homogeneous mound breakwater.

6. The proposed calibration method for VARANS models

This study describes a calibration method for the porosity, n_p, and the Forchheimer coefficients, α and β used in VARANS models to properly model the wave-porous structure interaction. The calibration method proposed in this study can be described as follows:

- *Step 1*: N_T physical tests using regular waves (H_{Ii}, T_i) are selected to calibrate the numerical VARANS model; $N_T = 25$ in this study.
- *Step 2:* Selection of the output variables to represent the wave-structure interaction; the squared coefficient of reflection, K_R^2, is selected in this study.
- *Step 3:* For each physical test ($i = 1, \ldots, N_T$), N_R numerical simulations are conducted using the VARANS model with a different combination of porosity and Forchheimer coefficients randomly selected in reasonable pre-determined ranges. In this study, $0.37 \leq n_p \leq 0.46$, $200 \leq \alpha \leq 20{,}000$ and $0.400 \leq \beta \leq 4.000$ for mound breakwaters, and $N_R = 15$. A total of N_T x N_R numerical cases are conducted using the VARANS model, and N_T x N_R numerical results of the output variables (K^2_{RVOF} in this study) are obtained.
- *Step 4:* A NN model is created, from the results of the available N_T x N_R numerical cases, to emulate the VARANS model. The NN model has five input variables (H_I, T, n_p, α,β) and, in this study, one output variable ($K^2_{R,NN}$). If the coefficient of determination of the NN estimations, K^2_{RNN}, compared to K^2_{RVOF} is $R^2 < 0.90$ (less than 90% of explained variance), then the N_R in *Step 3* should be increased.
- *Step 5:* Estimation of the output variable (*Step 2*) by the NN model created in *Step 4* are conducted to cover the complete range of n_p, α and β values. For each physical test {H_{Ii}, T_i } ($i = 1, \ldots, N_T$) used for calibration in *Step 1*, N_{np} porosities, N_α values of α, and N_β values of β are combined ($N_{np} = 19$, $N_\alpha = 200$ and $N_\beta = 721$, in this study) in a 3D space of {n_p, α, β}. A total of N_T x N_{np} x N_α x N_β (68,495,000 in this study) numerical cases are predicted by the NN model to calculate the K^2_{RNN} corresponding to each combination of {n_p, α, β} and each physical test {H_{Ii}, T_i}.
- *Step 6:* Calculation of the root-mean-square error, ε_{rms}, between the squared coefficient of reflection measured in physical tests, K^2_{RLAB}, and predicted by the NN model, K^2_{RNN}, corresponding to the N_T physical tests. The combination of {n_p, α, β} with the minimum ε_{rms} provides the recommended porosity, n_p, and Forchheimer coefficients (α and β) for the VARANS model.
- *Step 7:* If any recommended value of n_p, α or β in *Step 6* is the maximum or minimum value of the ranges considered in *Step 3*, the corresponding range should be widened to keep the optimum within the limits selected in *Step 3*.

In this study, the ranges of n_p, α and β were selected to cover all values found in the literature; however, the optimum combination of {n_p, α, β} was found for $\alpha = 200$, just in the limit of the range $200 \leq \alpha \leq 20{,}000$ considered in the literature. This fact is suggesting that some porous structures, such as the homogeneous mound breakwater considered in this study, may have a better combination of {n_p, α, β} with $\alpha < 200$. For this reason, *Step 2* recommends using a wider range for α, for example $100 \leq \alpha \leq 20{,}000$, than the range used in this study. This issue will be the subject of a future work.

The flow-chart in Fig. 10 summarizes the proposed calibration method for VARANS models. In this study, the calibration method is based on the proportion of reflected wave energy, K_R^2; however, this method can be applied to other representative variables (*Step 2*), such as overtopping, run-up, wave forces, etc. In these cases, the NN model (*Step 4*) may use a different o several output variables to better represent the wave-structure interaction. Note that the proposed calibration method must be applied for each layer of porous media forming the structure with its characteristic D_{n50} and a range of porosity values representative of the unit size. In this case the breakwater is a homogeneous and permeable mound breakwater with a single D_{n50} (m) = 0.03 and range $0.37 \leq n_p \leq 0.46$, which corresponds to the possible porosities for the size of the homogeneous stones.

To show the strength and the applicability of the proposed calibration method for Forchheimer coefficients, new IH-2VOF cases were simulated following the traditional methodology of the studies found in the literature (Table 1); that is: 2 wave conditions of {H_{I1} (m) = 0.03, T_1 (s) = 1.12} and {H_{I2} (m) = 0.10, T_2 (s) = 2.46}, two values of $\alpha = 200$ and 2000, and three values of $\beta = 0.8$, 1.5 and 3 were selected in combination with a fixed porosity $n_p = 0.46$ (the value physically measured in laboratory). Table 3 shows the results obtained in the IH-2VOF model by applying (1) 2 values of α and 3 values of β, and (2) the optimum combination {$n_p = 0.44$, $\alpha = 200$ and $\beta = 2.825$} obtained from the proposed calibration method. It is observed that for both wave conditions, the absolute error, ε_α , with the optimum combination {$n_p = 0.44$, $\alpha = 200$ and $\beta = 2.825$} is much smaller than selecting 2 values of α and 3 values of β. Moreover, with this method it is possible to calibrate the most suitable porosity for the porous media of the structure. The choice of 2 values of α and 3 values of β for two wave conditions does not represent the wave-structure performance for all laboratory tests; whereas the optimum combination obtained with the proposed calibration method does.

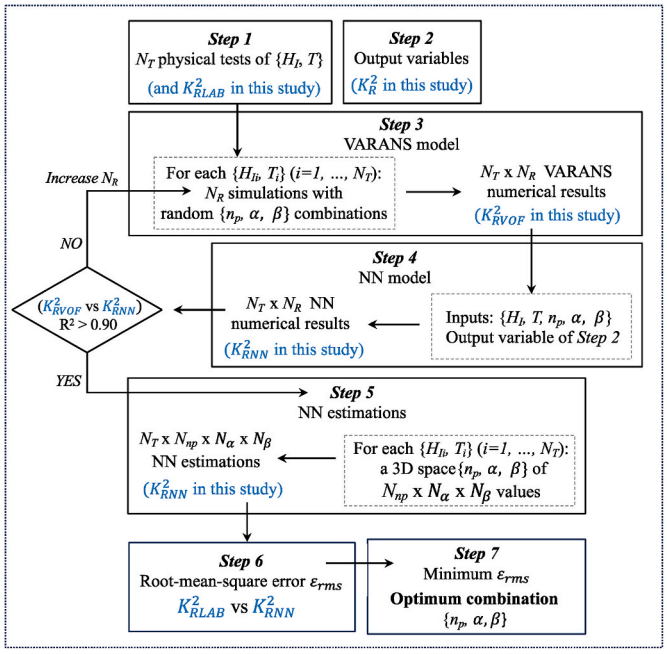

Fig. 10. Flow-chart of the proposed calibration method for VARANS models to calculate the optimum combination of n_p, α and β to model the wave-porous structure interaction.

Table 3
Comparison between the absolute error (Eq. (9)) obtained in the IH-2VOF model using the traditional methodology for calibration and using the calibration method proposed in this study: ε_a (%) of $\alpha = 200$, 2000; beta = 0.8, 1.5, 3; $n_p = 0.46$ (measured at laboratory) and ε_a (%) of the optimum combination {$n_p = 0.44$, $\alpha = 200$ and $\beta = 2.825$}.

H_1(m) = 0.03; T_1 (s) = 1.12; n_p = 0.46 (Lab measured)	ε_a (%) = $\lvert K^2_{RLAB} - K^2_{RVOF}\rvert \bullet 100$			
	β = 0.8	β = 1.5	β = 3	Optimum combination n_p = 0.44, $\alpha = 200$ and $\beta = 2.825$
$\alpha = 200$	3.1	2.6	1.4	0.31
$\alpha = 2000$	2.9	2.3	1.2	
H_2(m) = 0.10; T_2 (s) = 2.46; n_p = 0.46 (Lab measured)	ε_a (%) = $\lvert K^2_{RLAB} - K^2_{RVOF}\rvert \bullet 100$			
	β = 0.8	β = 1.5	β = 3	Optimum combination n_p = 0.44, $\alpha = 200$ and $\beta = 2.825$
$\alpha = 200$	14.6	11.6	5.8	0.05
$\alpha = 2000$	13.2	10.0	4.4	

6.1. VARANS and NN model validation

From the available 37 physical tests, $N_T = 25$ randomly selected tests, corresponding to $25 \times 15 = 375$ numerical cases from the IH-2VOF model, were used in this study to calibrate porosity and Forchheimer coefficients; the optimum combination of {n_p, α, β} was $n_p = 0.44$, $\alpha = 200$ and $\beta = 2.825$ (see Section 5). The remaining $37 - N_T = 12$ available physical tests, corresponded to $12 \times 15 = 180$ numerical cases from the IH-2VOF model, were used in this study for a blind test of the proposed calibration method for VARANS models in two ways:

(1) Validation of the NN model: new estimations of K^2_{RNN} were obtained with the NN model for the wave input parameters {H_I, T} corresponding to the 12 physical tests not used for calibration; the calibrated parameters ($n_p = 0.44$, $\alpha = 200$ and $\beta = 2.825$) were fixed. The comparison between the measured, K^2_{RLAB}, in the 12 physical tests used for validation and the new NN estimations K^2_{RNN}, lead to a root-mean-square error $\varepsilon_{rms} = 2.56\%$, slightly higher than $\varepsilon_{rms} = 2.28\%$ obtained during the calibration process ($N_T = 25$ tests).
(2) Validation of the IH-2VOF model: numerical results using IH-2VOF, K^2_{RVOF}, were obtained for the 12 additional physical tests taken for validation; the calibrated parameters ($n_p = 0.44$, $\alpha = 200$ and $\beta = 2.825$) were fixed. The comparison between the measured, K^2_{RLAB}, in the 12 physical tests used for validation and the new IH-2VOF numerical simulations, K^2_{RVOF}, lead to a root-mean-square error $\varepsilon_{rms} = 1.90\%$, slightly lower than $\varepsilon_{rms} = 2.28\%$ which were obtained during the calibration process ($N_T = 25$ tests).

The combination of $n_p = 0.44$, $\alpha = 200$ and $\beta = 2.825$, which was the result of the calibration method, was validated with new physical tests and performed well in both IH-2VOF and NN model. Numerical IH-2VOF estimations of K^2_R were better than NN estimations ($\varepsilon_{rms} = 1.90\% < 2.28\%$), but NN estimations require a much lower computational effort, which is adequate to calibrate the parameters of the porous media {n_p, α, β}.

6.2. An adequate number of physical tests for calibration

The numerical analysis of wave-structure interaction and other coastal problems using VARANS models usually has a high computational cost (time and resources), which are not always available. For studies using VARANS models in numerical flumes, this section analyzes the minimum number of tests needed to properly apply the calibration method proposed in this study. The calibration method described in Section 6 was applied with different number of tests N_T = [2, 4, 8, 12, 16 and 20], randomly taken from the 25 physical tests used for calibration, following the steps gathered in Fig. 10.

Fig. 11 represents the 5%, 50% and 95% percentiles of the root-mean-square error, ε_{rms}, given by Eq. (10) for different number of tests N_T = [2, 4, 8, 12, 16 and 20]. With a number of tests $N_T = 8$, the median error value was $\varepsilon_{rms} = 3.24$ % with a reasonably low variability, which is a small enough error to consider that the optimum combination of {n_p, α, β} provide the adequate parameters for the porous media of the homogeneous mound breakwater in the VARANS model. A number of tests $N_T < 8$, shown a median error of $\varepsilon_{rms} > 8.58$ % with a large variability; it is hard to believe that the optimum combination of {n_p, α, β} obtained with $N_T < 8$ was adequate to describe the porous media.

Fig. 12 shows the distribution of the $N_T = 4$ tests, within the 25 physical tests used for calibration (blue circles), with the lowest and highest value of ε_{rms}. It is observed that, for the case with the lowest ε_{rms} (the best case), the selection of {H_I, T} covered a wide range of wave periods, T, in the 2D space {H_I, T}, while the highest ε_{rms} (the worst case) covered a small range of T in the space {H_I, T}. If one is forced to use this calibration method with few available physical tests, the results found in this Section suggest selecting points {H_I, T} covering the full range of wave periods, T, used in the experiments. One should consider that NN models are usually very good interpolating but very poor extrapolating.

7. Summary and conclusions

The main objective of this study was to develop a calibration method for the porous media to properly model the interaction between waves and coastal structures in VARANS models. The proposed calibration method calculates the values of Forchheimer coefficients, α and β, and the porosity, n_p, from the results of a Neural Network (NN) model developed using physical and numerical tests. In this study, 37 physical tests using regular waves were conducted in the 2D wave flume of the University of Granada for a homogeneous mound breakwater under regular waves, non-overtopping and non-breaking wave conditions. Numerical tests were simulated in the IH-2VOF model, reproducing the 37 physical tests with regular waves {H_I, T}. The squared coefficient of reflection, related to the proportion of reflected wave energy, K^2_R, was selected as the variable to represent the wave-structure interaction. The numerical cases were selected to cover a range of porosities, n_p, characteristic to the porous media with a nominal diameter D_{n50} (m) = 0.03,

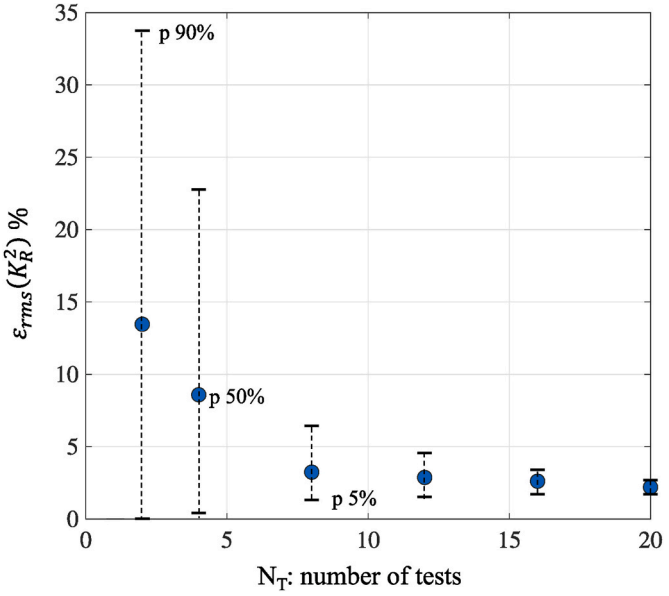

Fig. 11. Percentiles 5%, 50% and 90% of the root-mean-square error, $\varepsilon_{rms}(K^2_R)$ %, calculated by Eq. (10) for each number of test N_T.

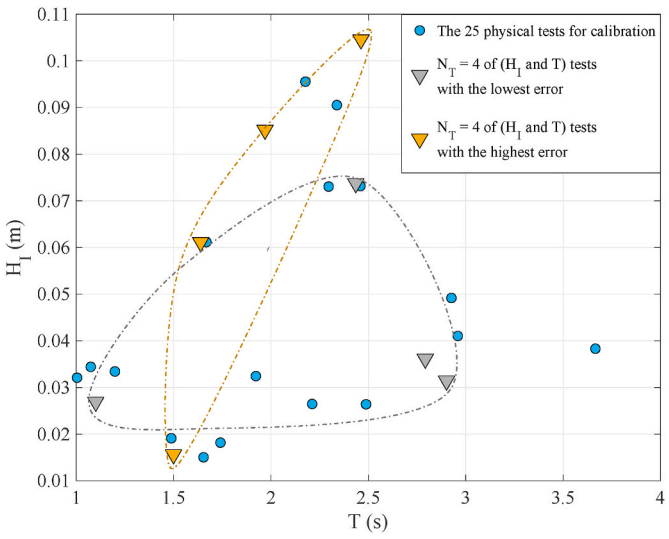

Fig. 12. Distribution of the $N_T = 4$ tests of H_I (y-axis) and T (x-axis) with the lowest (yellow triangles) and the highest (grey triangles) ε_{rms} value. Blue circles represents the 25 physical tests used for calibration.

and the ranges of Forchheimer coefficients, α and β, found in the literature. A total of 555 numerical cases using IH-2VOF were simulated. The results of 375 numerical cases using IH-2VOF were selected to develop a NN model with five input variables (H_I, T, n_p, α,β) and one output variable (K_R^2). Estimations of K_R^2 were obtained with the NN model to cover the complete range of n_p, α and β values found in the literature. The remaining 555–375 = 180 numerical cases of IH-2VOF were used to validate the proposed calibration method. The proposed calibration method was applied with different number of physical tests to obtain the minimum number of physical tests for calibration required to find adequate Forchheimer coefficients for the porous media in VARANS models.

The following conclusions are derived from this study:

1. The NN model developed with the input variables {H_I, T, n_p, α, β}, generate estimations K_{RNN}^2 which explained more than the 90% ($R^2 > 0.90$ and RMSE <5%) of the variance of the numerical K_{RVOF}^2 results obtained using IH-2VOF model. The NN model correctly emulated the IH-2VOF model and was a computationally efficient tool to predict numerical VARANS results.
2. The selection of one or a few physical tests {H_I, T} to calibrate the values of n_p, α and β for a general applicable model, as reported in the literature, is usually not sufficient to obtain an adequate representation of the wave-porous structure interaction. For the calibration of a VARANS model, applying or not the proposed calibration method, it is necessary to check the results obtained for each combination of {α, β} with many laboratory {H_I, T} tests.
3. The blind test conducted in this study resulted in a root-mean-square error $\varepsilon_{rms} = 2.56$ %, slightly higher than $\varepsilon_{rms} = 2.28$ % obtained during calibration. NN estimations, K_{RNN}^2, were in agreement with the numerical IH-2VOF calculations, K_{RVOF}^2, and the physical measurements, K_{RLAB}^2, when using the calibrated parameters: $n_p = 0.44$, $\alpha = 200$ and $\beta = 2.825$. The selection of a porosity, $n_p = 0.44$, and Forchheimer coefficients, $\alpha = 200$ and $\beta = 2.825$, was the optimum combination of {n_p, α, β} for the porous media of a homogeneous mound breakwater with D_{n50} (m) = 0.03 and under regular wave conditions.
4. In this study, 4 physical tests for calibration seem insufficient to obtain a combination of parameters {n_p, α, β}, which adequate represents the porous media in VARANS models. The selection of at least 8 physical tests for calibration leads to an adequate combination of {n_p, α, β} for VARANS modeling. If few physical tests are available for calibration, it is preferable tests {H_I, T} that cover the full ranges of T.
5. In this study, the optimum value of the linear Forchheimer coefficient was $\alpha = 200$, at the lower limit of the range of α values found in the literature ($200 \leq \alpha \leq 20{,}000$); therefore, the actual optimum combination of {n_p, α, β} may has an α lower than 200.

The proposed method based on a NN model is a robust, accurate and computational efficient tool to calibrate the porous media of a coastal structure under wave attack using VARANS models. This method not only obtains the optimum combination of Forchheimer coefficients {α, β}, but also estimates the actual porosity of the physical model, characterized by a nominal diameter D_{n50}. The correct calibration of a numerical model will allow proper analysis of the performance of wave-structure interaction and, once the model is setup, further physical phenomena and variations in the structure design can be studied. The proposed method may seem costly in time and money as it requires several steps (Step 1 to 7) and some laboratory tests (Step 1); however, the use of this calibration method and the numerical modelling (1) will be beneficial for the scientific and business community who need a very extensive laboratory test program to complete their studies; (2) will reduce the existing uncertainty in the numerical models calibration with a higher accuracy of obtaining the Forchheimer coefficients and the porosity. As a future work it would be interesting (1) to simulate a wider range for α, for example $100 \leq \alpha \leq 20{,}000$, than the range used in this study, and (2) to compare the results obtained by the proposed calibration method with the results of the NN methods of Vieira et al. (2021) and Dang et al. (2023) applied to the same physical model.

CRediT authorship contribution statement

Pilar Díaz-Carrasco: Conceptualization, Data curation, Formal analysis, Funding acquisition, Investigation, Methodology, Software, Validation, Visualization, Writing – original draft, Writing – review & editing. **Jorge Molines:** Conceptualization, Resources, Supervision, Writing – original draft, Writing – review & editing. **M. Esther Gómez-Martín:** Resources, Supervision. **Josep R. Medina:** Conceptualization, Formal analysis, Resources, Supervision, Writing – original draft, Writing – review & editing.

Declaration of competing interest

The authors declare that they have no known competing financial interests or personal relationships that could have appeared to influence the work reported in this paper.

Data availability

Data will be made available on request.

Acknowledgements

The first author is funded through the Juan de la Cierva 2020program (FJC 2020-044778-I) by "*Unión Europea – NextGenerationEU en el marco del Plan de Recuperación, Transformación y Resiliencia de España*", Spanish Ministry of Science and Innovation. This work is supported by two projects (1) PID 2021-126475OB-I00 and (2) PID 2021-128035OA-I00, funded by the MCIN/AEI/10.13039/501100011033 and, as appropriate, by " ERDF A way of making Europe", by the " European Union NextGenerationEU/PRTR". The authors thank Professor Javier L. Lara and the Environmental Hydraulics Institute of Cantabria (IH-Cantabria, Spain) for providing the IH-2VOF numerical model.

List of symbols

a	coefficient of the linear term of the drag force of Darcy-Forchheimer equation
b	coefficient of the non-linear term of the drag force of Darcy-Forchheimer equation
c_A	coefficient of the add mass of the inertial force of Darcy-Forchheimer equation
D_{n50}	nominal diameter of the porous media
f_b	body forces
F_{MT}	breakwater height
g	gravity
G_c	crest width
h	water depth
H_I	incident wave height for regular waves
I	hydraulic gradient
k	kinematic energy (turbulent model)
KC	Keulegan-Carpenter number
K_R^2	squared wave reflection coefficient
K_T^2	squared wave transmission coefficient
L	wavelength at the toe of the structure calculated with T
n_p	porosity
N_h	number of hidden layers
N_h	number of hidden layers
N_α	total number of α values simulated
N_β	total number of β values simulated
N_O	number of output layers
N_{np}	total of n_p values simulated
N_R	number simulations with a selection a random combination of α and β for each physical test
N_T	number physical tests
N_w	number of waves
p	wave pressure
P	number of parameters of the Neural Network model
$R_{e,c}$	porous Reynolds number
R^2	coefficient of determination
t	time
T	wave period
$\bar{u}$	wave velocity vector
U(0,1)	random number between [0,1]
α	linear Forchheimer coefficient
β	non-linear Forchheimer coefficient
$\Delta_\alpha, \Delta_\beta$	differential step of α and β coefficients, respectively
Δ_{np}	differential step of n_p values
Δ_x, Δ_y	cell size of the mesh grid in the x- and y-directions, respectively
ϵ	turbulent dissipation rate (turbulent mode)
ε_{abs}	absolute error
ε_{rms}	root-mean-square error
γ_p	add mass Forchheimer coefficient
ρ	water density
ρ_s	rock density
μ	dynamic water viscosity
ν	kinematic water viscosity

Subindexes “NN”, “LAB” and “VOF” represent the results obtained in the NN model, physical tests and IH-2VOF model, respectively
Subindexes “k”, “i” and “j” represent each n_p, {H_I, T} test, and pair of {α, β} values, respectively, simulated in the NN model
Subindex “r” represents the number of simulations with a random combination of n_p, α and β for each physical test

References

Baquerizo, A., 1995. Reflexión del oleaje en playas. Métodos de evaluación y de predicción (PhD thesis). University of Cantabria (Spain).

Beale, M.H., Hagan, M.T., Demuth, H.B., 2019. Deep Learning Toolbox -User's Guide. Matlab R2019a, Mathworks.

Burcharth, H.F., Andersen, O.K., 1995. On the one-dimensional steady and unsteady porous flow equations. Coast. Eng. 24, 233–257.

Camus, P., Tomás, A., Díaz-Hernández, G., Rodríguez, B., Izaguirre, C., Losada, I.J., 2019. Probabilistic assessment of port operation downtimes under climate change. Coast. Eng. 147, 12–24.

Clavero, M., Díaz-Carrasco, P., Losada, M.A., 2020. Bulk wave dissipation in the main layer of slope rock and cube armored breakwaters. J. Mar. Sci. Eng. 8 (3), 152.

CIRIA/CUR/CETMEF, 2007. The Rock Manual. The Use of Rock in Hydraulic Engineering, second ed. CIRIA, London (UK), p. C683.

Croquer, S., Díaz-Carrasco, P., Tamimi, V., Poncet, S., Lacey, J., Nistor, I., 2023. Modelling wave–structure interactions including air compressibility: a case study of breaking wave impacts on a vertical wall along the Saint-Lawrence Bay. Ocean. Eng. 273, 113971.

Dang, B.L., Nguyen-Xuan, H., Wahab, M.A., 2023. An effective approach for VARANS-VOF modelling interactions of wave and perforated breakwater using gradient boosting decision tree algorithm. Ocean. Eng. 268, 113398.

Del Jesus, M., Lara, J.L., Losada, I.J., 2012. Three-dimensional interaction of waves and porous coastal structures. Coast. Eng. 64, 57–72.

Díaz-Carrasco, P., 2019. Water-wave Interaction with Mound Breakwaters: from the Seabed to the Armor Layer. Ph.D. thesis. University of Granada (Spain).

Díaz-Carrasco, P., Moragues, M.V., Clavero, M., Losada, M.A., 2020. 2D Water-wave interaction with permeable and impermeable slopes: dimensional analysis and experimental overview. Coast. Eng. 158, 103682.
Díaz-Carrasco, P., 2023. Hydraulic performance analysis for homogeneous mound breakwaters: application of dimensional analysis and a new experimental technique. Ocean. Eng. 286, 115598.
Di Lauro, E., Lara, J.L., Maza, M., Losada, I.J., Contestabile, P., Vicinanza, D., 2020. Advantages of an innovative vertical breakwater with an overtopping wave energy converter. Coast. Eng. 159, 103713.
Di Lauro, E., Lara, J.L., Maza, M., Losada, I.J., Contestabile, P., Vicinanza, D., 2019. Stability analysis of a non-conventional breakwater for wave energy conversion. Coast. Eng. 145, 36–52.
Engelund, F.A., 1953. On the Laminar and Turbulent Flows of Ground Water through Homogeneous Sand. Danish Academy of Technical Sciences.
Ergun, S., 1952. Fluid flow through packed columns. Chem. Eng. Prog. 48 (2), 89–94.
Forchheimer, P., 1901. Wasserbewegung durch boden. Zeitschrift des Vereines Deutscher Ingenieuer, 45 edition.
García, N., Lara, J.L., Losada, I.J., 2004. 2-D Numerical analysis of nearfield flow at low-crested permeable breakwaters. Coast. Eng. 51, 991–1020.
Gu, Z., Wang, H., 1991. Gravity waves over porous bottoms. Coastal Eng. 15, 497–524.
Guanche, R., Iturrioz, A., Losada, I.J., 2015. Hybrid modeling of pore pressure damping in rubble mound breakwaters. Coast. Eng. 99, 82–95.
Guanche, R., Losada, I.J., Lara, J.L., 2009. Numerical modelling of wave loads for coastal structure stability. Coast. Eng. 56, 543–558.
Higuera, P., Lara, J.L., Losada, I.J., 2014. Three-dimensional interaction of waves and porous coastal structures using OpenFOAM. Part II: applications. Coast. Eng. 83, 259–279.
Hirt, C.W., Nichols, B., 1981. Volume of fluid (VOF) method for dynamics of free boundaries. J. Comput. Phys. 39, 201–225.
Hughes, S.A., 1993. Physical Models and Laboratory Techniques in Coastal Engineering, Advanced Series on Ocean Engineering. World Scientific.
Jensen, B., Jacobsen, N.G., Christensen, E.D., 2014. Investigations on the porous media equations and resistance coefficients for coastal structures. Coast. Eng. 84, 56–72.
Lara, J.L., del Jesus, M., Losada, I.J., 2012. Three-dimensional interaction of waves and porous coastal structures. Coast. Eng. 64, 26–46.
Lara, J.L., Ruju, A., Losada, I.J., 2011. Reynolds averaged Navier–Stokes modelling of long waves induced by a transient wave group on a beach. Proc. R. Soc. A 467, 1215–1242.
Lara, J.L., Losada, I.J., Guanche, R., 2008. Wave interaction with low-mound breakwaters using a RANS model. Ocean. Eng. 35, 1388–1400.
Lara, J.L., Garcia, N., Losada, I.J., 2006. RANS modelling applied to random wave interaction with submerged permeable structures. Coast. Eng. 53, 395–417.
Lin, P., 1998. Modelling of Breaking Waves. PhD Thesis. Cornell University.
Liu, P.L.F., Lin, P., Chang, K.A., Sakakiyama, T., 1999. Numerical modeling of wave interaction with porous structures. J. Waterw. Port, Coast. Ocean Eng. 125, 322–330.
Losada, I.J., Lara, J.L., Jesus, M., 2016. Modelling the interaction of water waves with porous coastal structures. J. Waterw. Port, Coast. Ocean Eng. 142 (6).
Losada, I.J., Lara, J.L., Guanche, R., González-Ondina, J.M., 2008. Numerical analysis of wave overtopping of rubble mound breakwaters. Coast. Eng. 55 (1), 47–62.
MATLAB, 2022. MATLAB®2022a. The MathWorks Inc. Natick, MA.
Mata, M.I., Van Gent, M.R., 2023. Numerical modelling of wave overtopping discharges at rubble mound breakwaters using OpenFOAM. Coast. Eng. 181, 104274.
Molines, J., Bayón, A., Gómez-Martín, M.E., Medina, J.R., 2020. Numerical study of wave forces on crown walls of mound breakwaters with parapets. J. Mar. Sci. Eng. 8 (4), 276.
Molines, J., Bayon, A., Gomez-Martin, M.E., Medina, J.R., 2019. Influence of parapets on wave overtopping on mound breakwaters with crown walls. Sustainability 11, 7109.
Moragues, M.V., Clavero, M., Losada, M.A., 2020. Wave breaker types on a smooth and impermeable 1:10 slope. J. Mar. Sci. Eng. (8), 296.
Norouzi, H., Bazargan, J., Azhang, F., Nasiri, R., 2022. Experimental study of drag coefficient in non-Darcy steady and unsteady flow conditions in rock fill. Stoch. Environ. Res. Risk Assess. 36, 543–562.
Palma, G., Formentin, S.M., Zanuttigh, B., Contestabile, P., Vicinanza, D., 2019. Numerical simulations of the hydraulic performance of a breakwater-integrated overtopping wave energy converter. J. Mar. Sci. Eng. 7, 38.
Pilechi, A., Baker, S., Cornett, A., 2018. Evaluation of a numerical wave modelling tool for studying the overtopping of rubble-mound breakwaters. In: Proceedings of the 7th International Conference on the Application of Physical Modelling in Coastal and Port Engineering and Science. Coastlab18.
Polubarinova-Kochina, P., 1962. Theory of Ground Water Movement. Princeton University Press, Princeton, NJ.
Reguero, B.G., Losada, I.J., Mendez, F., 2019. A recent increase in global wave power as a consequence of oceanic warming. Nat. Commun. 10, 205.
Sollitt, C.K., Cross, R.H., 1972. Wave transmission through permeable breakwaters. In: Proc., 13 International Conference on Coastal Engineering. ASCE, Vancouver, pp. 1827–1846.
Van Gent, M.R., 1995. Wave Interaction with Permeable Coastal Structures. Ph.D. thesis. Delft University.
Vieira, F., Taveira-Pinto, F., Rosa-Santos, P., 2021. Novel time-efficient approach to calibrate VARANS models for simulation of wave interaction with porous structures using Artificial Neural Networks. Ocean. Eng. 235, 109375.
Vílchez, M., Clavero, M., Losada, M.A., 2016a. Hydraulic performance of different non-overtopped breakwater types under 2D wave attack. Coast. Eng. 107, 34–52.
Vílchez, M., Clavero, M., Lara, J.L., Losada, M.A., 2016b. A characteristic friction diagram for the numerical quantification of the hydraulic performace of different breakwater types. Coast. Eng. 114, 86–98.
Wolters, G., van Gent, M.R.A., Allsop, W., Hamm, L., Muhlestein, D., 2010. In: HYDRALAB III: guidelines for physical model testing of rubble mound breakwaters, coasts. In: Marine Structures and Breakwaters: Adapting to Change: Proceedings of the 9th International Conference. Institution of Civil Engineers.
Zhao, P.-H., Sun, D.-P., Wu, H., 2021. Application of a VARANS based resistance-type porosity model on simulating wave interactions with perforated caisson sitting on a rubble-mound foundation. Appl. Ocean Res. 112, 102600.
Zhao, P.-H., Sun, D.-P., Wu, H., 2019. Investigation on A Resistance-Type porosity model and the experimental coefficients. China Ocean Eng. 33 (4), 468–476.